Morphological evolution and structural study of annealed amorphous-Ge films: Interplay between crystallization and dewetting

Sonia Freddi, Gianfranco Sfuncia, Michele Gherardi, Giuseppe Nicotra, Chiara Barri, Luca Fagiani, Mohammed Bouabdellaoui, Alexey Fedorov, Stefano Sanguinetti, Dominique Chatain, et al.

Morphological evolution and structural study of amorphous-Ge based nanostructures obtained by dewetting instability

Sonia Freddi[1], Gianfranco Sfuncia[2], Michele Gherardi[3], Giuseppe Nicotra[2], Chiara Barri[3], Luca Fagiani[3], Mohammed Bouabdellaoui[4], Alexey Fedorov[1], Dominique Chatain[5], Stefano Sanguinetti[1,6], Marco Abbarchi[4,7], Monica Bollani[1*]

[1] *Istituto di Fotonica e Nanotecnologie-Consiglio Nazionale delle Ricerche (IFN-CNR), LNESS laboratory, Como, Italy*
[2] *Istituto per la microelettronica e microsistemi- Consiglio Nazionale delle Ricerche (IMM-CNR), Catania, Italy*
[3]*Department of Physics, Politecnico di Milano, Milan, Italy*
[4] *Aix Marseille Univ, Université de Toulon, CNRS, IM2NP Marseille, France*
[5]*Aix-Marseille Univ, CNRS, CINaM, 13009 Marseille, France*
[6] *Dipartimento di Scienze dei Materiali, Università Milano Bicocca, Milano, Italy*
[7] *Solnil, 95 Rue de la République, Marseille, 13002, France*
[*]*Corresponding author: monica.bollani@ifn.cnr.it*

Abstract

In this work, the dewetting process of an amorphous-Ge-based thin film (a-Ge) upon annealing has been studied, highlighting the morphological and structural properties of the dewetted islands. By a combination of in-situ reflection high-energy electron diffraction (RHEED) during low and high-temperature annealing and by electron back scatter diffraction (EBSD), the initial crystallization dynamics of the Ge film has been clarified, and the structural characterization of the dewetted islands has been disclosed by high-resolution transmission electron microscopy (HR-TEM), atomic force microscopy (AFM) and scanning electron microscopy (SEM). Chemical composition has been assessed by electron energy loss spectroscopy (EELS). Different initial a-Ge film thickness (range: 10 nm - 200 nm) and annealing treatments, i.e. annealing temperature in the range between 600°C – 820°C, and annealing time in a 5 – 120 minutes range, have been investigated to control the dewetting process. Finally, we extended the solid state dewetting process up to 20 cm wafers showing the possibility to tune particles size varying the initial a-Ge thickness of the deposited film, highlighting the scalability of the process. Beyond fundamental understanding of the a-Ge dewetting process, these results are relevant for the fabrication of large-scale hard masters for nanoimprinting lithography and novel photonic platforms fabricated via a scalable, lithography-free, CMOS-compatible process.

Keywords

Dewetting, amorphous germanium, Ge islands, thin germanium film

Introduction

Dewetting is a shape instability shared by thin films of liquids and solids, occurring in particular condition of temperature and pressure, for which the thin films tend to agglomerate forming smaller structures. Thin solid films under perturbations, such as high pressure or high temperature, transform into isolated islands or, when using pre-patterned template, into complex nano-architectures. In order to minimize surface and interfacial energies, the metastable thin solid films can rupture and collapse into particles with a shape dependent on the particle-substrate contact angle at temperatures significantly below the melting temperature of the bulk phase [1]. The main physical mechanism at the basis of dewetting in solids is mass transport mediated by surface diffusion: atoms on the film surface move away from the edges leading to retraction, bulging, finger formation and finally, breaking of the film, into isolated islands [2,3,4,5]. Unlike top-down methods, one of the main advantages of this process is the possibility to functionalise a surface with nanostructures in a timeframe that depends only on the film thickness and not on the sample dimension, achieving low-cost devices for several applications such as high-density magnetic recording media, photocatalysis or sensors [6,7,8,9]. Among the dewetted systems reported in the literature, crystalline silicon-on-insulator (SOI) films have been largely studied. They have been considered as a model system for studying Si-based solid state (SSD) dewetting and exploiting in a plethora of photonics applications [10,11,12,13,14]. Spontaneous and patterned dewetting, indeed, are shown to allow the formation of dielectric Mie-resonators, featuring several resonant modes in the visible spectrum and representing alternative to plasmonic nanoparticles to manipulate light-matter interactions. Moreover, Si-based dewetted wires splitting, inter-connections and directions are studied: by engineering the dewetting fronts and exploiting the spontaneous formation of kinks, a Si-based field- effect transistor with state-of the-art trans-conductance and electron mobility is also achieved [15]. More recently, SiGe dewetting, i.e. $Si_{70}Ge_{30}$ dewetted structures directly formed on an electrically insulating and optically transparent substrate [16], has been efficiently exploited to realize arrays of nanostructures with typical footprint ranging from few nm up to several μm [17,18,19,20,21]. In the case of lens-like shaped SiGe particles, indeed, the effects of Mie resonances and far-field light focusing were demonstrated using Raman microscopy and spectroscopy. Considering that Ge-based photonic devices work at near and mid-infrared frequency, the study and validation of a low-cost processing of SSD for the Ge films is also of great interest for applications. This is also true when considering the large geometrical aspect ratio (AR = H/D, where H is the island height and D is its diameter) of the final equilibrium shape of pure Ge islands with respect to Si or $Si_{70}Ge_{30}$ islands (AR (Ge) ~ 0.8-1, AR (Si or SiGe) ~ 0.20-0.6) [19]. For

instance, this latter feature of Ge is favourable for the formation of a strong magnetic dipole mode Mie resonance, unlike what found in Si dewetted inslands, where electric and magnetic dipole modes are overlapped owing to the underlying low AR of the Si islands. Furthermore, thanks to its lower atom binding energy, Ge dewetting can be achieved at sensibly lower temperature with respect to Si extending the processability of this material to simpler experimental setups. In spite of the relevance of this material for photonic devices, the structural investigation of its dewetted state/process is not yet complete. Recent works on Ge thin films showed qualitatively different typologies of dewetting using different thicknesses of an initial layer of Ge [22,23,24,25]. These authors generally report that the dewetting is initiated at about 580–700 °C, depending on germanium thickness and cleaning process. The appearance of surface undulation is first observed, leading to the particle formation and the rupture of Ge layers by narrow channels or rounded holes in the layers with the thicknesses of 10–60 and 86 nm, respectively [22]. The channel widths are significantly narrower than the distance between the particles that causes the formation of thinned Ge layer areas between particles at the middle dewetting stage. Here we confirm this morphological evolution of Ge-based thin films, highlighting moreover the structural properties of dewetted Ge-based islands, using a wide range of thicknesses (from 10 nm to 200 nm) and the scalability of the dewetting process. By a combination of in-situ reflection high-energy electron diffraction (RHEED) and by electron back scatter diffraction (EBSD) after high-temperature annealing we clarify the initial crystallization dynamics of the amorphous Ge film. We complete the analysis by the structural characterization of the dewetted islands (ex situ, post-annealing) by high-resolution transmission electron microscopy (HRTEM), energy electron loss spectroscopy (EELS), atomic force microscopy (AFM) and scanning electron microscopy (SEM). Different initial amorphous film thickness (spanning from 10 nm to 200 nm) and annealing treatments are investigated to control the dewetting process of Ge film. To confirm the capability to control the dewetting process, Ge-based islands are demonstrated over 200 mm wafer, corroborating the scalability of this low-cost process for novel technological applications.

Materials and methods

The initial step is the growth by molecular beam epitaxy (MBE) of germanium films on 25 - 60 nm of SiO_2 thermal oxide film deposited by chemical vapour deposition on a Si (001) substrate. Different thicknesses of Ge (specifically 10 nm, 25 nm, 50 nm and 200 nm) are deposited at 120°C at a growth rate of 0.25nm/s, achieving amorphous germanium (a-Ge) films. The initial phase is amorphous, as shown by in situ RHEED analyses where diffraction rings are absent. Different annealing treatments are then carried out, varying the temperature and the time of annealing to

study and optimize the dewetting process. The annealing treatments are performed in UHV conditions in a dedicated custom-made annealing machine, at a pressure down to 10^{-9} mbar and a temperature increment rate of 10K/s. In detail, temperature up to 900°C can be reached by a halogen lamp (maximum power: 400 W) and the ramp used to achieve the desired temperature is managed by an automatic controller. AFM measurements are performed to monitor the evolution of the film roughness at different annealing steps, correcting the measured corrugation profile from the AFM tip convolution effects. This is accomplished by using an internal calibration standard (gold nanoparticles) for *in situ* calibration of the AFM tip radius and to monitor changes in tip size. All AFM images are acquired in tapping mode, using a super-sharp silicon probe (typical radius of curvature 2 nm) and processed with align rows-median to remove skipping lines using the Gwyddion software. The same software is employed to extrapolate the filling factor (FF, defined as the ratio between area covered by dewetted structures and the total surface) and the size distribution, using the high resolution-SEM planar view images. The structural characteristic of the dewetted Ge nanostructures is finally determined by HR-TEM, using a high-angle annular dark-field scanning transmission electron microscopy (HAADF-STEM) with a collection angle β that ranges from 80 to 174 mrad, and a convergence semi-angle α=10 mrad. This configuration is selected to acquire highly-sensitive Z-contrast images, where brighter contrast corresponds to higher Ge content [26]. Chemical composition has been measured during the HRTEM analyses by EELS detector. Finally, the thick 200 nm Ge film is heated in ultra-high vacuum, and after cooling, an EBSD investigation has been performed on the sample. This technique is used to determine the orientations of the crystals on the amorphous silica layer.

Results

At first, the morphological evolution upon annealing of a 10 nm thick a-Ge (amorphous Ge) layer has been studied: the annealing treatment has been performed in a temperature range between 600°C and 800°C, and for different durations, ranging from 5 minutes up to more than 60 minutes.

The AFM measurements are mainly exploited to monitor the evolution of the film roughness at different annealing steps (Figure 1). The root mean square roughness (RMS) shows an increasing trend from 0.2 nm (Figure 1-a) to 1.4 nm after a five minute annealing at 600° C (Figure 1-b). In Figure 1-c, acquired on a sample annealed for 15 minutes at 600°C, it is possible to observe a change in the morphological features of the surface: while dark spots appear (voids), also features with a higher height start to form (brighter spots).

Figure 1-d,e report the topographic features of the samples annealed for 15 minutes at 750°C and for more than 15 minutes at 800°C, respectively. In the latter case, in detail, annealing time of the

sample whose image is reported was 30 minutes. It is worth to point out that considering a time range varying from 15 to 60 minutes, the surface of the a-Ge layer does not undergo any damage related to silicon diffusion or germanium desorption, but it always appears as in the shown panels (e, j).

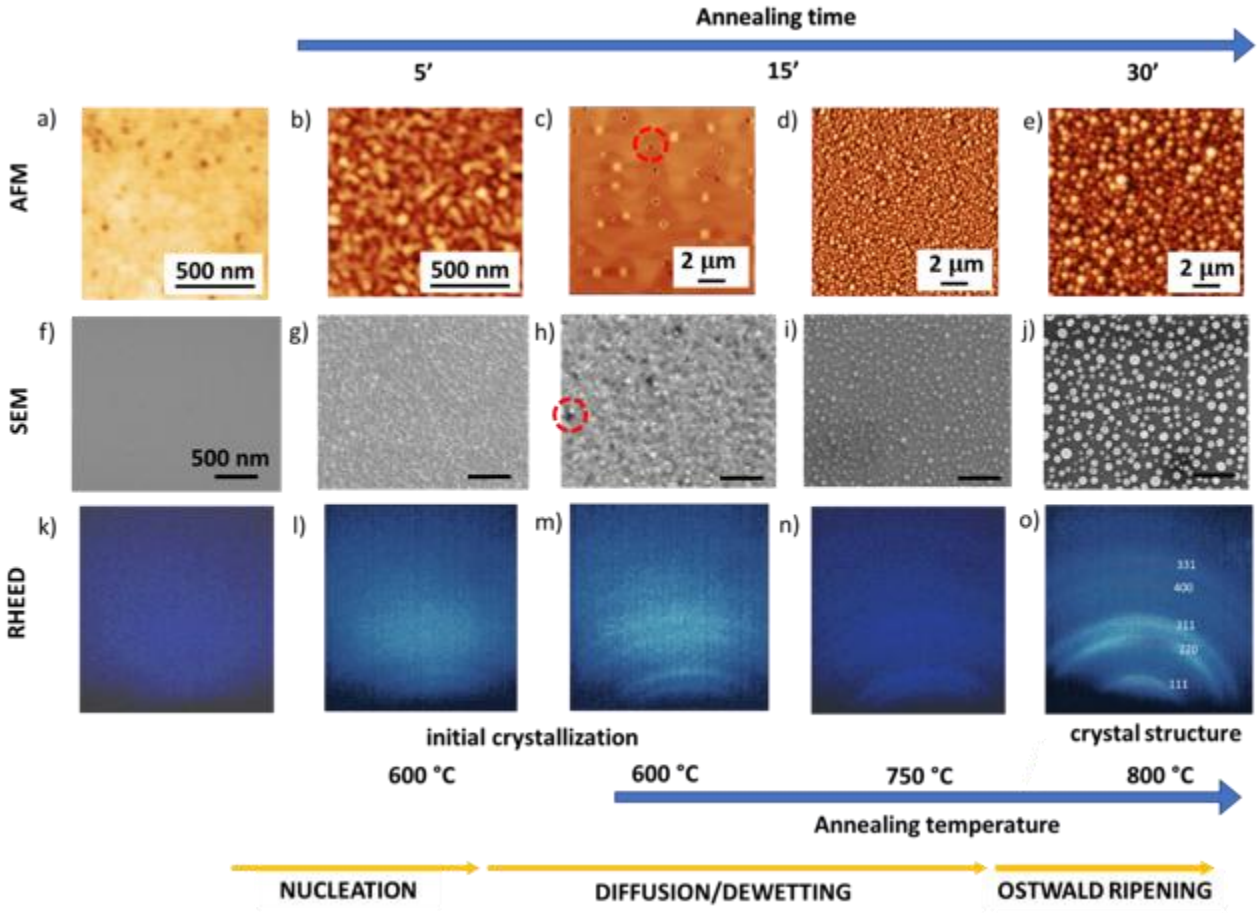

Figure 1: Morphology evolution of 10 nm a-Ge during the annealing procedure. AFM topography images acquired on the a) as deposited a-Ge film, with a surface roughness of 0.2 nm; b) the sample after 5 minutes of annealing at 600°C, with a surface roughness of 1.4 nm; c) the Ge film after annealing for 15' at 600°C; d) the Ge film annealed for 15' at 750°C, and e) the Ge film after annealing for 30' at 800°C. Planar view SEM images of the a-Ge sample as deposited f) and annealed for: g) 5 minutes at 600°C; h) 15 minutes at 600°C, i) 15 minutes at 750 °C, j) 30 minutes at 800°C. RHEED acquired on the a-Ge sample before annealing k), and RHEED diffraction patterns taken respectively: l) after 5 minutes at 600°C; m) after 15 minutes at 600°C; n) after 15 minutes at 750°C; o) after 30 minutes at 800°C. Of note: red circles in panel c) and h) enlightened the voids formation.

The SEM analyses confirm this scenario (Figure 1-f,g,h,i,j). Initially a flat surface is observed (Figure 1-f), then corrugations on the upper Ge layer are visible in Figure 1-d: at the longer annealing time, more Ge atoms move and are incorporated in the islands, accentuating the waviness of the film surface. Spontaneous dewetting starts with the heterogeneous nucleation of voids forming at randomly distributed defects, followed by void opening (Figure 1-h); at the bottom of the voids the SiO_2 substrate appears as dark grey spots, highlighted by a dotted red circle in Figure 1-h. A further increase of the annealing temperature to 750°C, and for a same annealing time of 15 minutes, leads to a complete Ge nano-island formation, without residual a-Ge layer between the islands (Figure 1-i).In the case of the Si based crystalline films, the Si<110>-oriented fronts are stable and dewet with a greater velocity than the unstable fronts, forming elongated structures called Si fingers and where the mass of the film is efficiently transferred [15]. On the contrary, in the case of a-Ge films no fingers formation is observed, excluding a preferential stable dewetting fronts. Increasing the temperature up to 800°C, the surface-driven forces lead to the

coarsening between separated nano-islands (Figure 1-j). Regarding the crystallinity, no diffraction rings are visible for the film surface before annealing (Figure 1-k), and the first diffraction rings are observable at ~600°C (Figure 1-l): increasing the annealing time, more visible diffraction rings are detected, confirming the formation of the crystal seeds (Figure 1-m). Significant changes in the crystallinity are not observed between annealing at 650°C and 750°C, for 15 minutes (Figure 1-m,n), but after 30 minutes of annealing at ~800°C, the RHEED diffraction patterns, which correspond to the (111), (220), (311), (400) and (331) crystallographic planes, clearly appear as reported in Figure 1-o. To further confirm the crystallinity and the material quality after the annealing treatment, the HR-TEM analyses are carried out. These analyses are performed on two different Ge film thicknesses, 10 nm and 50 nm. The samples are annealed at different temperatures, considering that to dewet thicker films it is generally necessary to increase the temperature and/or the annealing time. The relative structural characterizations of the first sample annealed at ~750°C for 15 minutes are reported in Figure 2. The HR-TEM cross section analysis highlights the non-homogeneity of dimensions and shapes of the Ge crystalline structures but excludes the presence of a residual Ge layer between the islands (Figure 2-a). For the largest islands, the contact angles are in the range of 110°-120° (Figure 2-b), the islands are crystalline although they contain structural defects as visible in Figure 2-c. HR-TEM characterization on the sample annealed at 800°C for 15 minutes (Figure 3-a) shows monocrystalline Ge islands with a contact angle up to ~ 90° degrees and a slight Ge depression in the SiO_2 film (see Figures 3-b, c). The depression is due to the high temperature used during the annealing process, for which Ge nanostructure sinks into the softer SiO_2 layer [27,28]. The chemical maps obtained by EELS confirm that during the annealing treatment silicon did not diffuse from the SiO_2 layer into the Ge islands (Figure 4).

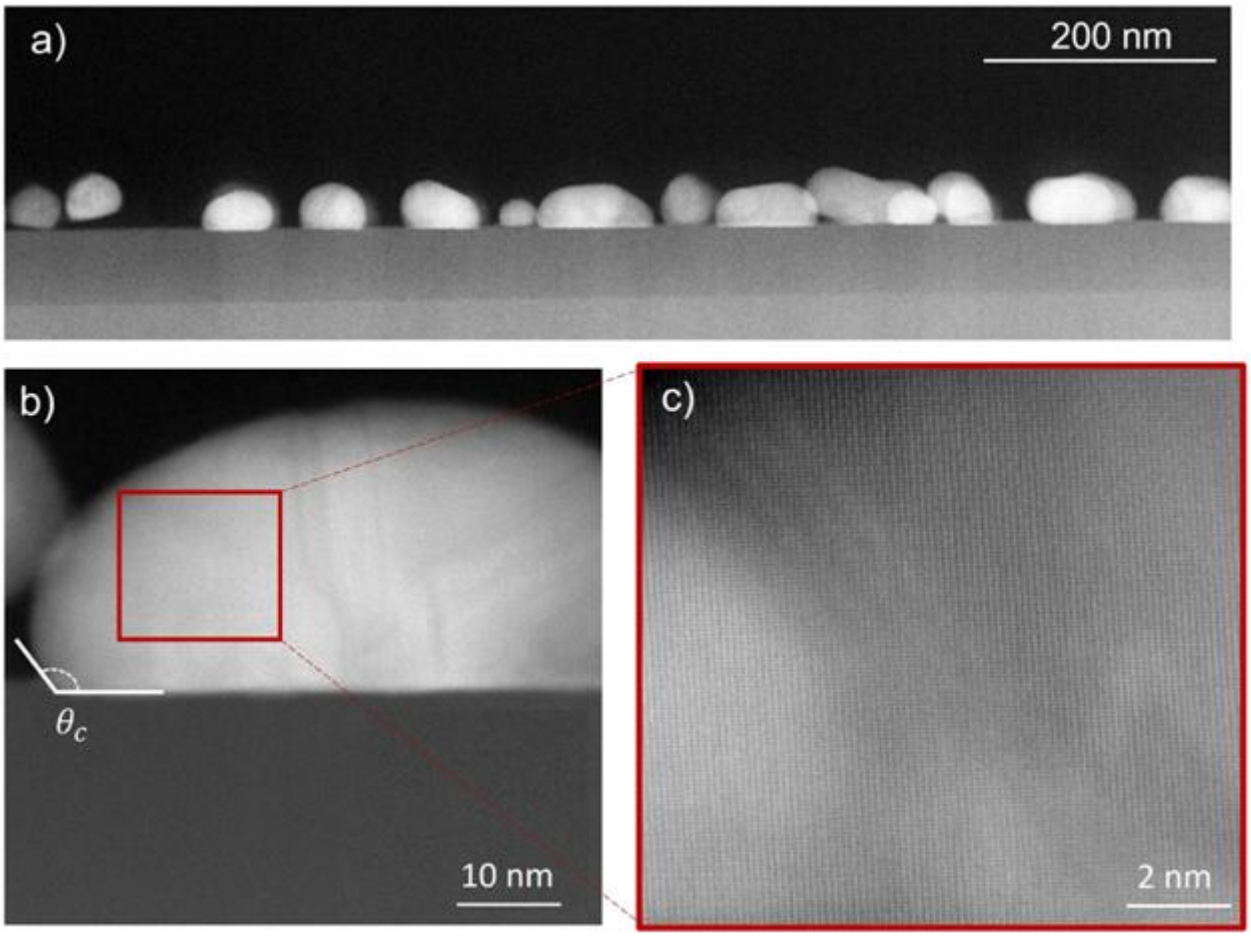

Figure 1. a) STEM image of Ge crystalline island, originally 10nm thick, obtained by the annealing treatment of 15 minutes at ~ 750°C. b) HR-TEM image of one Ge island, where a contact angle of 113° -120° degrees us highlighted. c) Zoomed inset of the Ge island where the crystalline structure and defects are observable.

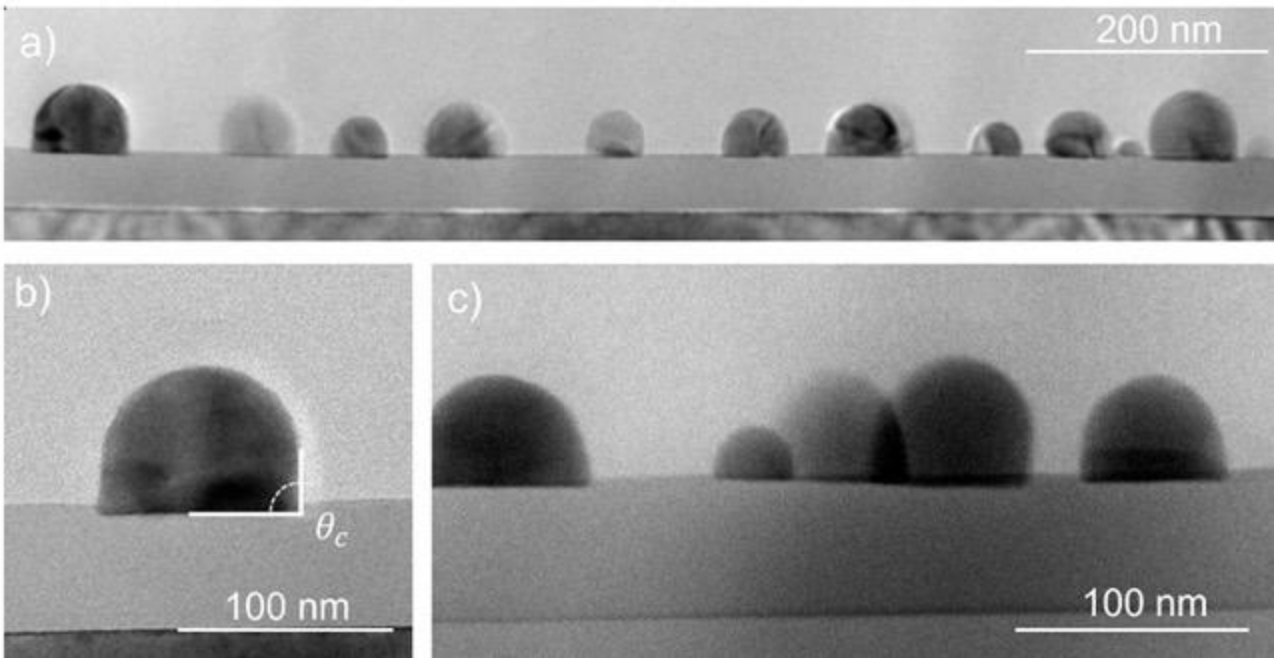

Figure 3: a) TEM image of Ge crystalline island, originally 50nm thick, obtained by the annealing treatment of 15 minutes at 800°C. b) Reduction of the contact angle up to 90°degrees ±5°. c) light depression of the Ge islands in the SiO2 bulk substrate, confirmed by EELS analysis reported in figure 4.

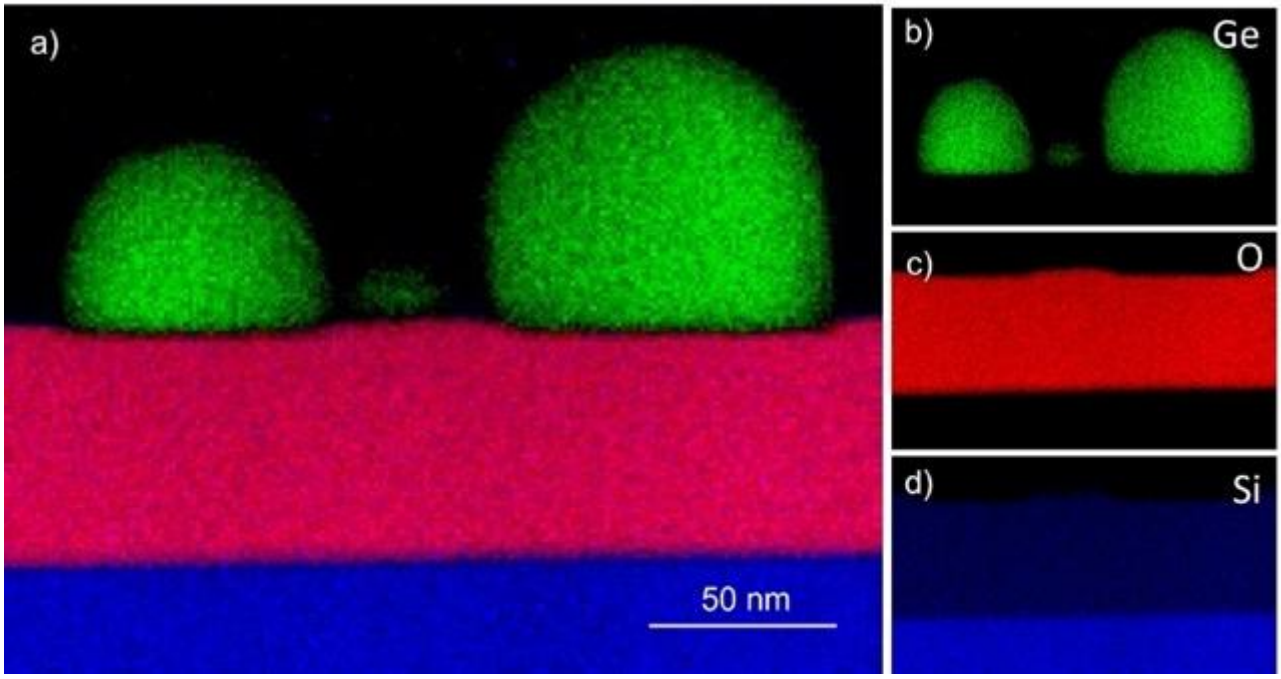

Figure 4 a) EELS chemical map of the Ge island dewetted at 800°C for 15 min, from an original film thickness of 50 nm. b) - c) - d) chemical maps of single contribution of germanium, oxygen, silicon respectively. Two depressions zone in O and Si areas corresponding to the location of Ge islands could be observed in c) and d).

Using thicker a-Ge layers, higher annealing temperature and longer annealing time can help to better understand the dewetting mechanism. Indeed, it is known that these parameters play a crucial

a)

Sample	T (°C)	Time (min)
A	750	30
B	750	90
C	750	120
D	800	30
E	800	90
F	800	120
G	820	30
H	820	90
I	820	120

b)

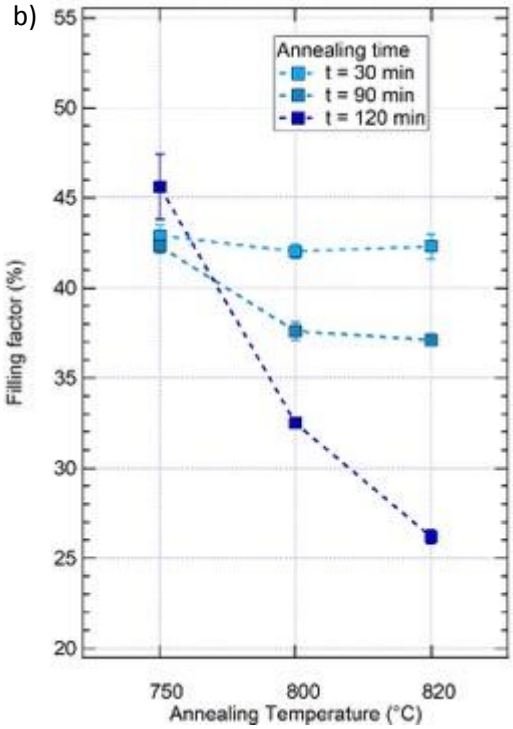

Figure 5: a) *Annealing time and temperature for the A-I studied samples. b) Filling factor (FF) evaluated on the A-I samples. a-Ge thickness is 25 nm for all samples.*

role in the homogeneity, size distribution and crystallinity of the islands [24]; thus 9 samples (all ~25 nm thick and referred to as A-I in Figure 5-a) have been studied. The annealing has been performed in a custom-made chamber, varying the temperature between 750°C and 820°C, and the annealing time between 30 and 120 minutes.

Figure 6 gathers the SEM images collected on the A-I samples, as function of annealing time (horizontal) and temperature (vertical). The filling factor (FF) has been evaluated considering several images acquired on the A-I samples. As noticed in Figure 5-b, for each annealing temperature, increasing the annealing time leads to a lower FF, excepted for the experiments at T = 750°C, where the FF is almost constant. At constant annealing time, the FF decreases as the annealing temperature increases, excepted for the samples annealed for 30 minutes, where the FF remains almost constant at about 42%.

The size distribution of the nano-islands in the A-I samples has been reported in Figure 7. For almost all samples (A, C, D, F, G, H, I) a bimodal distribution is observed, as often reported in the literature [22, 29], therefore we fitted all the distributions with two Gaussian functions.

Let us start comparing the A-B-C samples series, annealed at 750°C. Well-defined nano-islands of Ge without residual amorphous Ge between the sites have already formed after 30 minutes. As

previously mentioned, increasing the annealing time from 30 to 120 minutes does not significantly influence the FF, but changes the size distribution. The average diameters of the two distributions of sample A annealed for 30 mins and sample B annealed for 90 minutes are almost the same, while the ratio between the two Gaussians heights (□) halves, indicating that the smallest Ge islands have merged into larger ones.

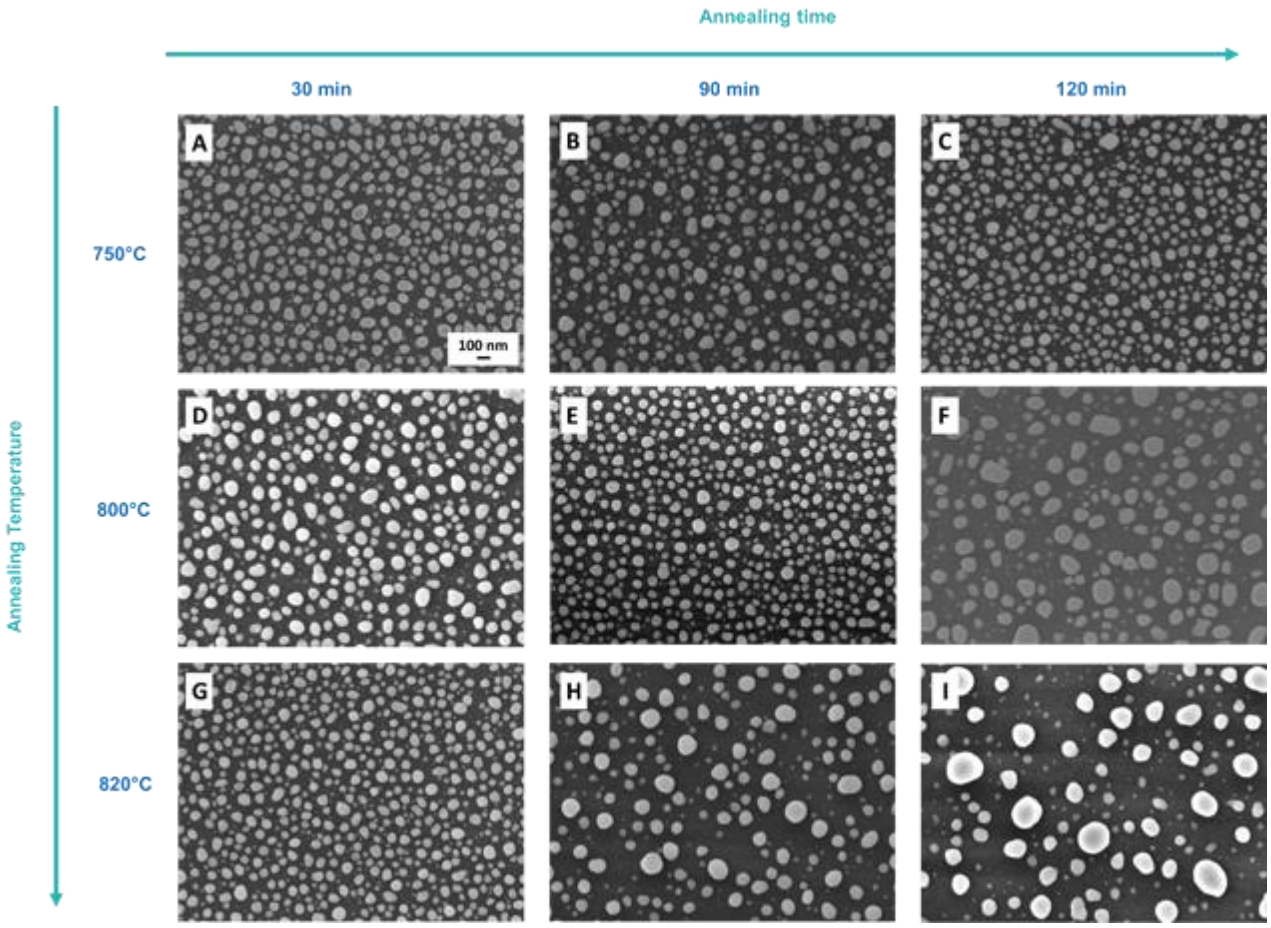

Figure 6: SEM images acquired in planar view of samples A-I as function of three different annealing time (horizontal) and three annealing temperatures (vertical). Time and temperature are indicated in the figure. The scale bar is the same for all images.

Increasing the annealing time to 120 minutes (sample C) leads to an increase in the average diameters of the larger islands and a further decrease of □. Then, comparing D-F and G-I samples, annealed at 800°C and 820°C respectively, shows that a longer anneal leads to the coarsening between separated nano-islands (Figure 6) and to the increase in the average diameter (Figure 7). This is consistent with the decrease of the FF values (Figure 5-b). Both samples' series present a similar behaviour in terms of α: an increase of anneal durations from 30 mins (D and G) to 90 mins (E and H) produces the decrease of α, indicating that, for longer annealing time, islands with an average diameter between 45 nm and 65 nm increase in number compared to smaller islands (size around 10-20 nm). After a 120 minute anneal (F and I), α increases again, the width of the second

Gaussian also significantly increases, and its position is shifted to larger width, indicating a stronger coarsening of separated nano-islands. When comparing results for the different annealing temperature at a fixed annealing time, in all sample series (A-D-G, B-E-H and C-F-I), an increase in the average size of the Ge islands is observed at higher annealing temperature (Figure 7). We conclude that an increase in the annealing temperature leads to the progressive disappearance of the smaller nano-islands, due to a large mass transfer towards the larger islands as descripted by Ostwald ripening [23].

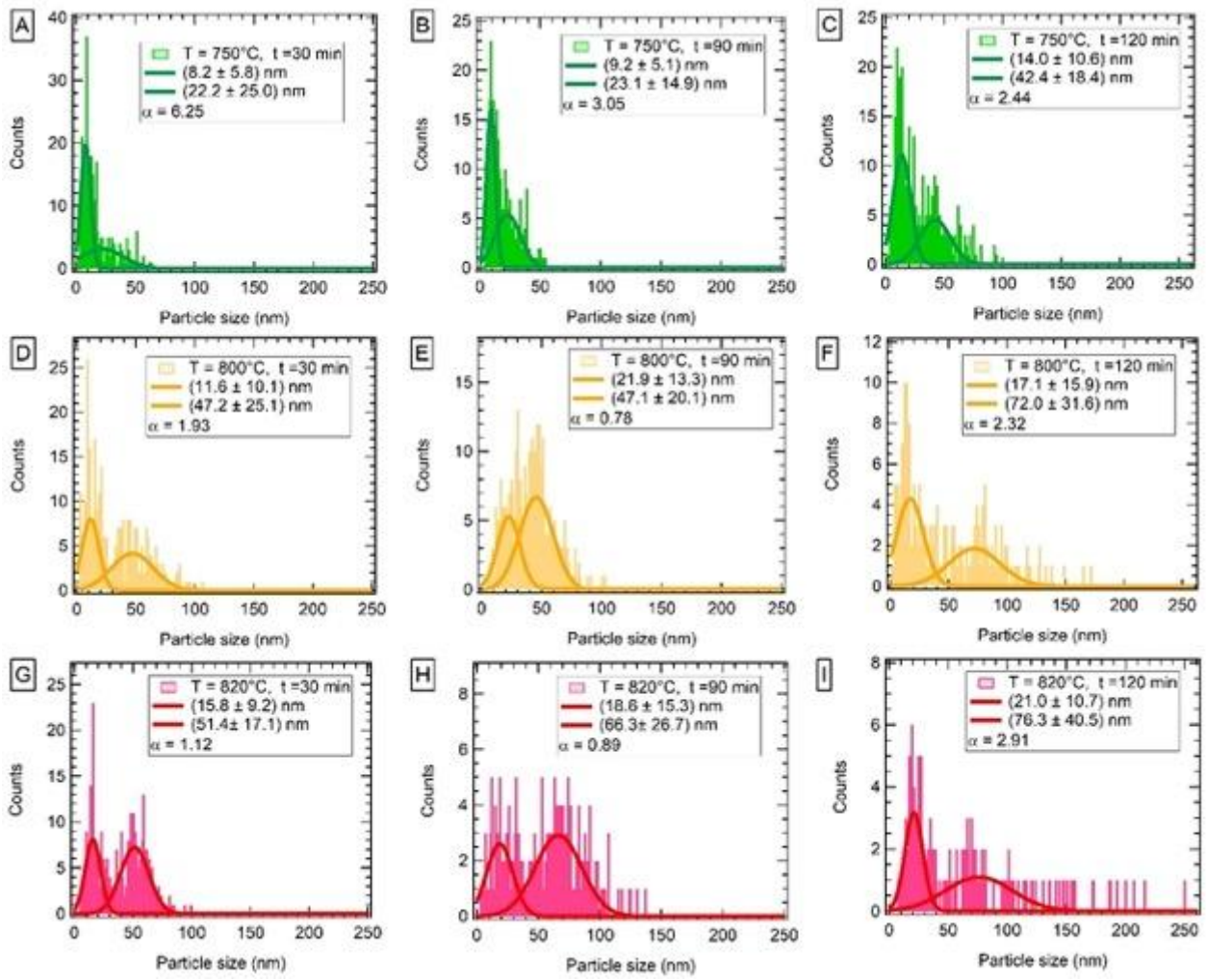

Figure 7: Size distribution of islands in samples A-I as function of annealing time (horizontal) and annealing temperature (vertical). Time and temperature are indicated in the captions of each graph. A same scale for the particle size has been adopted to help in making comparison among the samples.

To further probe the morphology evolution, electron backscatter diffraction (EBSD) analyses are performed using a thicker a-Ge film (200 nm) deposited on thermal SiO_2 via MBE. This Ge larger film thickness has been chosen to obtain grains with larger dimensions and to validate the SSD process observed on thick amorphous films. This topic has been scarcely studied up to date; indeed, no work exploiting Ge layers thicker than 80-100 nm to investigate SSD has been so far published. To the best of our knowledge, there is only one paper [22] reporting on the creation of

submicrometric Ge islands via SSD from 10-86 nm thick Ge layers as a function of the annealing temperature. The possibility to tune the size of the dewetted islands from a few hundred nm to one micrometer could allow to use these nanostructures arrays both as a support for Mie resonances at longer wavelength or as photonic platform for the biological system sensing.

A sample containing larger grains allows to analyse by EBSD the crystalline features of the Ge grains obtained from an amorphous Ge film on an amorphous silica substrate upon annealing. Figure 8 presents the results obtained on one sample after annealing at 750°C for 120 minutes. A SEM top view image of the sample (Figure 8-a) reveals a completely dewetted stage, with Ge islands of a size ranging from 1 to 3 µm. Figure 8-b is an inverse pole figure (IPF-Z) of a region containing several hundred Ge grains viewed in the z-direction, perpendicular to the substrate. It shows that the Ge crystals tends to have a (110) plane parallel to the substrate (4.4 times more frequent than a random orientation distribution). In Figure 8-d, EBSD confirms that most of the Ge-islands are single-crystal but some of the grains are made of several crystals. A further EBSD analysis allows to find that the crystals inside a single island are mainly in twinned relationships. The EBSD analysis of this sample confirms the results acquired on thinner films and provide new information on the crystallography of the Ge grains formed on amorphous silica: there is a weak preference for one of the lowest surface energy orientations to be parallel to the substrate (110) [30]. There is no in-plane alignment of the crystals on the amorphous substrate. Moreover, a large majority of the grain boundaries inside the multi-crystalline grains are twin boundaries.

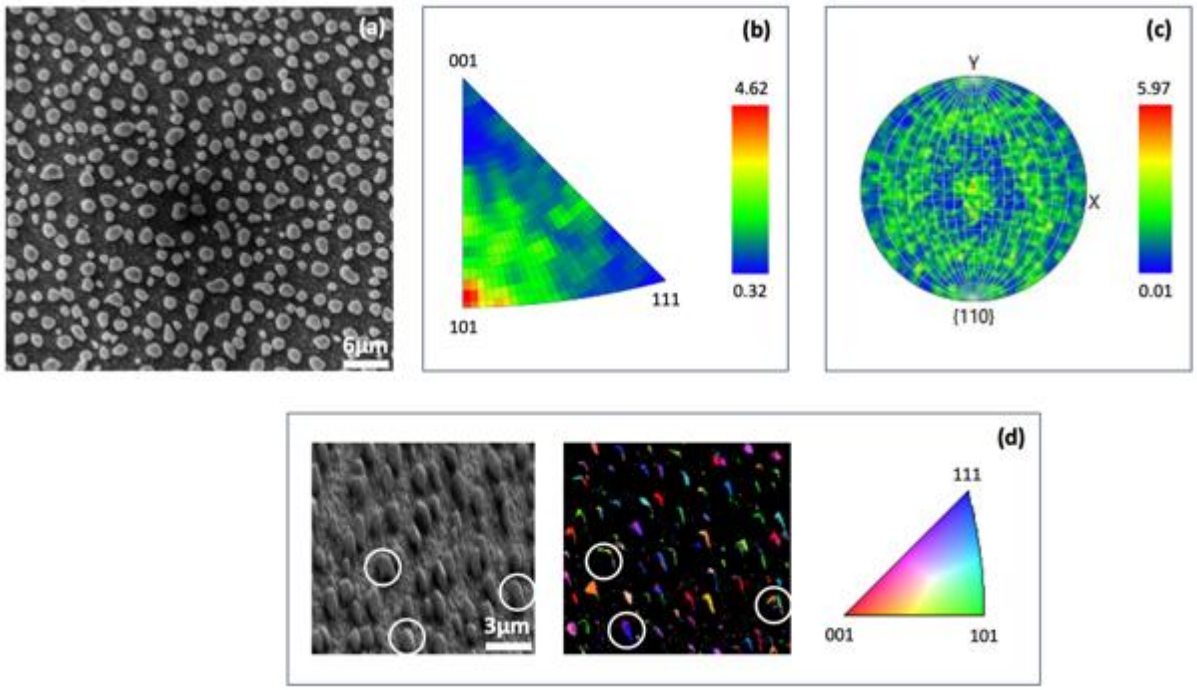

Figure 8: (a) SEM images of the view on a top of a 200 nm – a-Ge layer annealed at 750°C for 120 mins. (b) Ge IPF-Z showing a preferred Ge orientation with a (110) plane parallel to the substrate. In (c) the (110)PF shows there is no preferential alignment

within their interfacial plane on the amorphous silica layer because it prevents Ge to see the Si crystal underneath. In (d) a 70°-tilted electron image together with an IPF-Z image coloured according to the standard stereographic triangle scheme. The Ge grains surrounded with white circles are polycrystalline. Further EBSD analysis allows to find these crystals are mostly in twinned orientation relationship. Of note: since the image is acquired tilted, the spherical islands appear elliptical.

Finally, we report on the fabrication of Ge-based islands over 8 inches (200 mm) wafer via solid-state dewetting, representing a record scale size for semiconductor dewetting, accounting for the scalability of the process. The fabrication of the samples proceeds as previously described in the material and methods section. The sample is heated to temperature between 720°C to 800° C for a duration from 30 to 60 minutes depending on the film thickness, longer times are required for thicker a-Ge film. Pictures of three different 200 mm wafers bearing isolated Ge-islands are displayed in Figure 9.

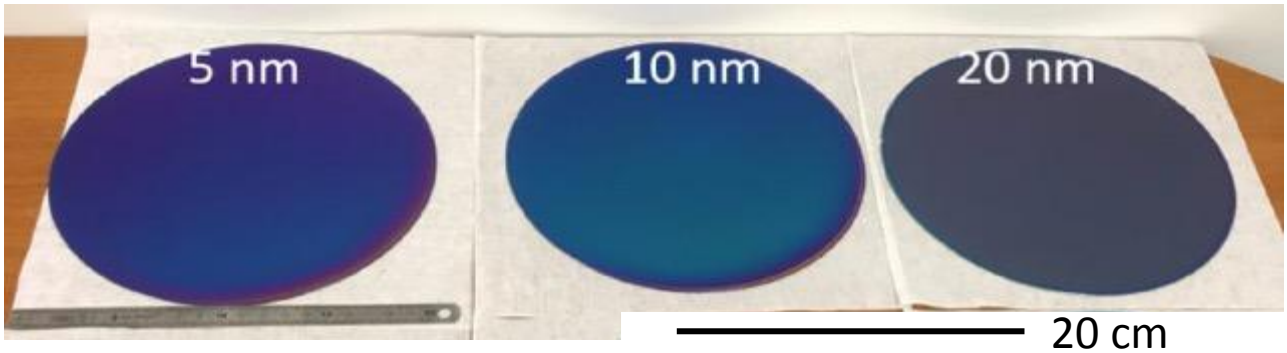

Figure 9: images of the three different 20 cm Si(001) wafer, on which three different layers of germanium (5 nm, 10 nm and 20nm) are deposited and then annealed in the MBE chamber. A ruler is placed under the first wafer to highlight the size of the wafer.

The homogeneity of the dewetted structures is tested on a wafer bearing isolated islands (10 nm of a-Ge dewetted for 1 hour at 800° C). The wafer is broken in small parts, analysed by SEM (Figure 10). These parts are about 2 cm apart one from the other and cover an area of 2 cm x 2 cm. They are labelled 1-1 to 3-3 depending on their position in a 3 x 3, square matrix. Statistical distribution of particles size is obtained from each SEM image. The analysis (not shown) demonstrates that, within a relatively large particle size distribution, the investigated areas are rather homogeneous and

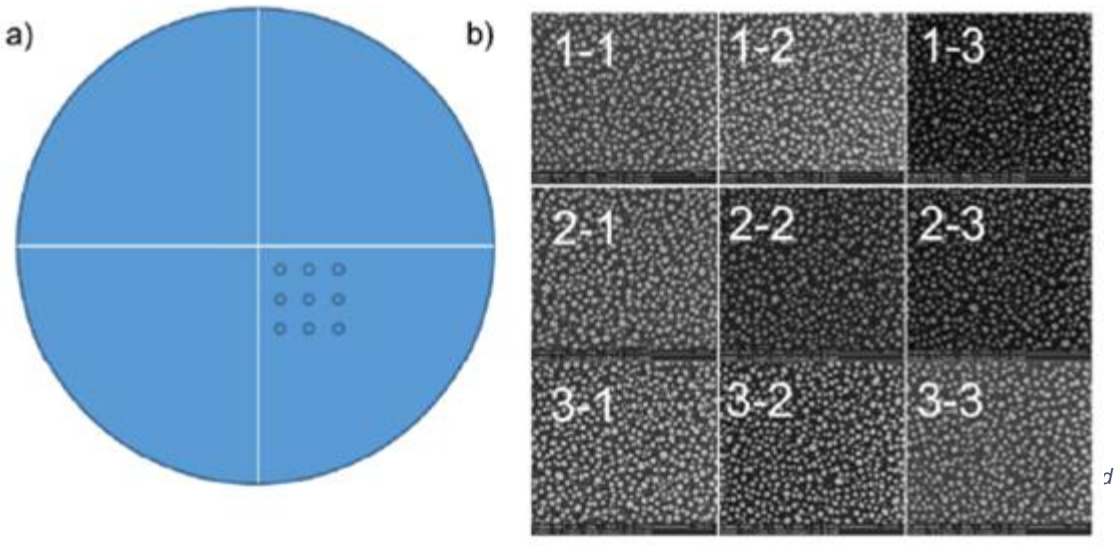

providing an average island diameter of 63 nm with a fluctuation around the average of about 17 nm.

Discussion

The morphological evolution under annealing of an amorphous Ge thin layer on SiO_2 is a process that can be partially related to solid state dewetting. Indeed, as it has been previously reported, two different aspects should be considered in the formation of crystalline Ge islands upon annealing of an amorphous Ge layer: (i) the energy required for the crystallization of the material (thermodynamic aspect) and (ii) the surface energy minimization by (surface) diffusion (kinetic aspect) [23]. For thin layers, as reported in Figure 1, the first significant change in surface morphology is due to the crystallization of the amorphous layer at temperatures around ~ 600 °C. At this temperature, crystal seeds form in preferential regions within the amorphous Ge film, and the Ge atoms of the amorphous parts of the film move toward these seeds causing the increase of surface roughness. This phenomenon starts after 5 min and is clearly observable after 15 min of annealing, where the crystalline Ge seeds have increased their dimensions and the (very local) diffusion of the Ge atoms around them has started to leave uncovered regions of the SiO_2 substrate. This evolution mechanism from amorphous to crystalline phase agrees with the observed RHEED diffraction patterns. During the first annealing step, a very weak diffraction pattern signal is observed in compliance with the first crystal seeds formation. When crystallization is completed, the formation of crystals (of different orientations) corresponds to a strong signal detected in diffraction. The temperature detected for the crystallization process (600°C) is significantly higher than the 300°C detected by Wakayama et al [29] but comparable with the data reported in [22,24,31]. The discrepancy noted in the crystallization temperature is already known in literature; indeed, different annealing temperature (ranging from ~600°C up to ~800°C) have been reported, mainly due to the uncertainty of the temperature calibrations, the chamber residual pressure in which the dewetting process starts, as well as the different thicknesses of the original germanium film. However, the activation of surface diffusion, and crystallization processes require surface Ge oxide degassing as a first step, which takes place at ~500°C. By increasing the annealing temperature, the diffusion mechanisms dominate, and polycrystalline Ge structures are formed (Figure 1). Initially the shape of the Ge nanostructures is hemispherical. The measurements of the angles obtained in Figure 2 can be compared to the angles corresponding to the Young equation:

$$\cos\theta_C = \frac{\gamma_{SiO2} - \gamma_{Ge/SiO2}}{\gamma_{Ge}} \quad \text{[eq01].}$$

where the γ_{Ge} is usually found in the range between 1.32 J/m^2 and 1.71 J/m^2, depending on the crystalline orientation of the surface, and, as previously done in refs [24,32] we can consider an average value of 1.5 J/m^2; the substrate contribution (γ_{SiO2}) is 0.4 J/m^2 [33], whereas the interface term $\gamma_{Ge/SiO2}$ is in the range between 1 J/m^2 and 0.6 J /m^2 [24,32,33]. The corresponding Young angle values (ϑ) are in the range of 110°-120° that correspond to the value range measured on cross-view HR-TEM image in Figure 2. This value is also close to 106° calculated for liquid Ge on silica [34] and consistent with the fact that the physical state of the metal barely changes the contact angle. At higher annealing temperature, around 800°C, the island density decreases with respect to the increase of temperature can be ascribed to the coarsening mechanism associated to the Ostwald ripening phenomena [35]. The geometry of the 3D dewetted structures formed at high temperature present a reduction of the "apparent" contact angle (of about ~ 30°) partly due to the formation of a depression of the interface level Ge/SiO_2 (Figure 4-c, d), when the crystal adopts a lens equilibrium shape [27,28].

The depression areas on the silica substrate have already been observed with Si islands, which underwent a long or high-temperature annealing treatment [36,37]. Ge islands during high temperature annealing treatments undergo a similar process: as reported in ref [22], volatile SiO and GeO molecules are formed by the reaction occurring at the triple line between SiO_2, Ge and the vapour phase:

$$SiO_{2(solid)} + Ge_{(solid)} = SiO_{(gas)} + GeO_{(gas).}$$

In the case of thicker Ge films, the mechanisms involved are similar to the ones already described, although annealing time and temperature required to achieve complete dewetting are different. In particular, in the case of the 25 nm a-Ge samples investigation, the longer annealing time (120 minutes) coupled with the higher temperatures (800°C and 820°C) enhanced the Ostwald ripening between the Ge islands, leading to a significative higher peak position of the size distribution.

Regarding the size distribution, the bimodal trend has been previously observed and described for a-Ge [22, 29], for a-Si [29] and $Si_{1-x}Ge_x$ [38] films. The bimodal size distribution could depend on different parameters, such as the initial layer thickness, the annealing temperature, and the rate at which the annealing temperature has been achieved, whereas the annealing time does not seem to play a crucial role in the distribution shape [22]. In particular, at first the dewetting process begins from the formation of large Ge particles from the voids and areas of thinned Ge layer between them. These areas then turn into groups of smaller Ge particles after the annealing at intermediate temperature (i.e. 750°C, in our case). As already mentioned, when the annealing is performed at higher temperatures (i.e. 800°C or 820°C), the smaller islands tend to agglomerate, enhancing the Ostwald ripening phenomenon, in agreement with what reported in Ref. [22].

The role of initial layer thickness has been thoroughly investigated in Ref. [29]. The crystallization of the islands and their size distribution have been explained considering the change in the free energy, which strongly depends on the initial layer thickness.

In particular, the formation of islands which size distribution is bimodal arises from a two-step crystallization procedure. Initially, crystallite agglomeration initiates once they achieve a critical radius to minimize the total energy. During this phase, the islands exhibit a quite uniform radius. Subsequently, through additional thermal annealing, crystallization concludes, resulting in small islands. The key observation is that, by leveraging the influence of the Ge/SiO_2 interface, significant size uniformity of the islands can be achieved under relatively mild thermal annealing conditions.

Increasing the annealing time, the Oswald ripening process becomes dominant, leading to the formation of larger islands.

Additionally, a thick 200 nm film shows consistent behaviours with the thinner film. It gives the opportunity to do EBSD analysis on a statistically representative collections of Ge grains. It confirms a close to random orientation relationship of the Ge crystals/grains on silica, with a weak preference of grains growing with a (110) plane parallel to the substrate, a plane which has a low surface energy but not the minimum one (which would be (001)). Such orientation could be related to the presence of the surface oxide layer or of the oxide substrate. However, this shows that the orientation of the grains is probably not influenced by the substrate during crystallization of the a-Ge film. On the other hand, the EBSD analysis has allowed to show that many of the grain boundaries within the crystalline Ge grains are twin grain boundaries.

Conclusion

In summary, the formation of Ge nano-islands through a dewetting process has been studied, following the morphological and structural evolution of a-Ge films of different initial thicknesses (i.e. from 10 nm up to 200 nm). We have assessed that spontaneous dewetting starts from the random nucleation of voids, during an annealing at 600°C for 5 minutes. Increasing the annealing temperature and time, complete the formation of Ge islands. The effect of different annealing treatments (temperature and time) has been thoughtfully investigated. RHEED, STEM and EBSD investigations reveal the crystalline nature of the Ge islands, whereas the chemical composition is assessed by EELS. In agreement with what has already been published by other authors [22,23,24,25], these characterizations show that the amorphous Ge films dewet into Ge crystalline nano-islands with dynamics dominated by crystallization of the amorphous material into crystalline nano-seeds and material transport at Ge islands. Surface energy minimization determines the

dewetting process of crystalline Ge and controls the final stages of the process. At very high temperatures, coarsening of the island size distribution is observed. In particular, two different aspects are relevant in the formation of crystalline Ge islands upon annealing of an amorphous Ge layer, which are only partially related to solid-state dewetting: the energy required for the crystallization of the material (thermodynamic aspect) and the surface diffusion energy minimization (kinetic aspect). Finally, we extended the solid state dewetting process up to 200 mm wafers showing the possibility to tune particle size (by tuning the initial thickness of the deposited film) and the possibility to use these dewetted samples as master for nanoimprinting lithography as reported in ref [39].

Funding. This research was funded by the project CNR "EPOCALE" (2022-2024), European Commission (grant n° 828890), by "AGRITECH" project (Centro Nazionale per le Tecnologie dell'Agricoltura, Finanziato dall'Unione europea – Next Generation EU -PNRR 2022-25), by PRIN2022 PNRR "ACONITE" (Finanziato dall'Unione europea – Next Generation EU, grant n° P2022HRTYH). S.F, M.G. and M.B. acknowledge Polifab, the micro and nanofabrication facility of Politecnico di Milano, for supporting the devices characterization.

References

[1] C.V. Thompson, Solid-State Dewetting of Thin Films, Annu. Rev. Mater. Res. 42 (2012), 399.

[2] Y.A. Shin, C.V. Thompson, Templated fingering during solid state dewetting, Acta Materialia, 207 (2021), 116669

[3] F. Leroy, F. Cheynis, Y. Almadori, S. Curiotto, M. Trautmann, J.C. Barbé, P. Müller, How to control solid state dewetting: A short review, Surface Science Reports 71.2 (2016), 391-409.

[4] B. Bhatt, S. Gupta, V. Sumathi, S. Chandran, K. Khare, Electric Field Driven Reversible Spinodal Dewetting of Thin Liquid Films on Slippery Surfaces, Adv. Mater. Interfaces 10 (2023), 2202063. DOI: 10.1002/admi.20220206

[5] L.-X. Lu, Y.-M. Wang, B. M. Srinivasan, M. Asbahi, J. K. W. Yang, Y.-W. Zhang, Nanostructure Formation by controlled dewetting on patterned substrates: A combined theoretical, modeling and experimental study, Scientific Reports 6 (2016), 32398. DOI: 10.1038/srep32398

[6] Y. J. Oh, C. A. Ross, Y.S. Jung, Y. Wang, C. V. Thompson, Cobalt Nanoparticle Arrays Made by Templated Solid-State Dewetting, Small 5 (2009), 860. doi.org/10.1002/smll.200801433

[7] N. T. Nguyen, M. Altomare, J. Yoo, P. Schmuki, Efficient photocatalytic H_2 evolution: controlled dewetting–dealloying to fabricate site- selective high- activity nanoporous Au particles on highly ordered TiO_2 nanotube arrays, Advanced Materials 27(20) (2015), 3208-3215. doi: 10.1002/adma.201500742.

[8] J. Ye, D. Zuev, S. Makarov, Dewetting mechanisms and their exploitation for the large-scale fabrication of advanced nanophotonic system, International Materials Reviews 64(8) (2018), 439-477. doi.org/10.1080/09506608.2018.1543832

[9] M. Altomare, N. T. Nguyen, P. Schmuki, Templated dewetting: designing entirely self-organized platforms for photocatalysis. Chemical science 7(12) (2016), 6865-6886. doi: 10.1039/c6sc02555b

[10] M. Naffouti, R. Backofen, M. Salvalaglio, T. Bottein, M. Lodari, A. Voigt, T. David, A. Benkouider, I. Fraj, L. Favre, A. Ronda, I. Berbezier, D. Grosso, M. Abbarchi, M. Bollani, Complex dewetting scenarios of ultrathin silicon films for large-scale nanoarchitectures, Science advances 3.11 (2017), eaao1472.

[11] F. Cheynis, F. Leroy, P. Müller, Dynamics and instability of solid-state dewetting, C. R. Physique 14 (2013), 578–589, doi.org/10.1016/j.crhy.2013.06.006

[12] D. Toliopoulos, M. Khoury, M. Bouabdellaoui, N. Granchi, J.B. Claude, A. Benali, I. Berbezier, D. Hannani, A. Ronda, J. Wenger, M. Bollani, M. Gurioli, A. Sanguinetti, F. Intonti, M. Abbarchi, Fabrication of spectrally sharp Si-based dielectric resonators: Combining etaloning with Mie resonances, Opt. Express 28 (25) (2020), 37734-37742. doi.org/10.1364/OE.409001

[13] M. Abbarchi, M. Naffouti, B. Vial, A. Benkouider, L. Lermusiaux, L. Favre, A. Ronda, S. Bidault, I. Berbezier, N. Bonod, Wafer Scale Formation of Monocrystalline Silicon-Based Mie Resonators via Silicon-on-Insulator Dewetting, ACS Nano 8(11) (2014), 11181–11190. https://doi.org/10.1021/nn505632b

[14] M. Abbarchi, M. Naffouti, M. Lodari, M. Salvalaglio, R. Backofen, T. Bottein, A. Voigt, T. David, J.B. Claude, M. Bouabdellaoui, A. Benkouider, I. Fraj, L. Favre, A. Ronda, I. Berbezier, D. Grosso, M. Bollani, Solid-state dewetting of single-crystal silicon on insulator: effect of annealing temperature and patch size, Microelectronic Engineering 190 (2018), 1-6. https://doi.org/10.1016/j.mee.2018.01.002

[15] M. Bollani, M. Salvalaglio, A. Benali, M. Bouabdellaoui, M. Naffouti, M. Lodari, S. Di Corato, A. Fedorov, A. Voigt, I. Fraj, L Favre, J. B. Claude, D. Grosso, G. Nicotra, A. Mio, A. Ronda, I. Berbezier, M. Abbarchi, Templated dewetting of single-crystal sub-millimeter-long nanowires and on-chip silicon circuits, Nat Commun 10 (2019), 5632.

[16] A. Benali, J.-B. Claude, N. Granchi, S. Checcucci, M. Bouabdellaoui, M. Zazoui, M. Bollani, M. Salvalaglio, J. Wenger, L. Favre, D. Grosso, A. Ronda, I. Berbezier, M. Gurioli, M. Abbarchi, Flexible photonic devices based on dielectric antennas, Journal of Physics: Photonics 2 (2020), 015002. https://doi.org/10.1088/2515-7647/ab6713

[17] N. Granchi, M. Montanari, A. Ristori, M. Bouabdellaoui, C. Barri, L. Fagiani, M. Gurioli, M. Bollani, M. Abbarchi, F. Francesca Intonti, Near-field hyper-spectral imaging of resonant Mie modes in a dielectric island, APL Photonics 6.12 (2021), 126102.

[18] L. Fagiani, N. Granchi, A. Zilli, C. Barri, Francesco Rusconi, Michele Montanari, Erfan Mafakheri, M. Celebrano, M. Bouabdellaoui, M. Abbarchi, F. Intonti, A. Khursheed, P. Biagioni, M. Finazzi, M.A. Vincenti, M. Bollani, Linear and nonlinear optical properties of dewetted SiGe islands, Optical Materials: X, 13 (2022), 100116.

[19] N. Granchi, L. Fagiani, M. Salvalaglio, C. Barri, A. Ristori, M. Montanari, M. Gurioli, M. Abbarchi, A. Voigt, M. A. Vincenti, F. Intonti, M. Bollani, Engineering and detection of light

scattering directionalities in dewetted nanoresonators through dark-field scanning microscopy, Opt Express 31(5) (2023), 9007-9017. https://opg.optica.org/oe/abstract.cfm?doi=10.1364/OE.481971

[20] A. A. Shklyaev, A. E. Budazhapova, Submicron- and micron-sized SiGe island formation on Si(100) by dewetting, Thin Solid Films 642 (2017), 345 - 351. https://doi.org/10.1016/j.tsf.2017.09.045

[21] N. Granchi, L. Fagiani, C. Barri, A. Federov, M. Abbarchi, M.A. Vincenti, F. Intonti, M. Bollani, Light scattering features induced by residual layers in dielectric dewetted nanoparticles, Opt. Mater. Express 13 (2023), 3394-3404.

[22] A.A. Shklyaev, A. V. Latyshev, Dewetting behavior of Ge layers on SiO_2 under annealing, Scientific Reports 10, 13759 (2020). https://doi.org/10.1038/s41598-020-70723-6.

[23] D. Toliopoulos, A. Fedorov, S. Bietti, M. Bollani, E. Bonera, A. Ballabio, G. Isella, M. Bouabdellaoui, M. Abbarchi, S. Tsukamoto, S. Sanguinetti, Solid-State Dewetting Dynamics of Amorphous Ge Thin Films on Silicon Dioxide Substrates, Nanomaterials 10(12) (2020), 2542.

[24] C. Dabard, A.A. Shklyaev, V.A. Armbrister, A.L. Aseev, Effect of deposition conditions on the thermal stability of Ge layers on SiO_2 and their dewetting behavior, Thin Solid Films 693 (2020), 137681.

[25] I. Berbezier, M. Aouassa, A. Ronda, L. Favre, M. Bollani, R. Sordan, A. Delobbe, P. Sudraud, Ordered arrays of Si and Ge nanocrystals via dewetting of pre-patterned thin films, J. Appl. Phys, 113 (6) (2013), 064908.

[26] M. Bollani, D. Chrastina, V. Montuori, D. Terziotti, E. Bonera, G. M. Vanacore, A. Tagliaferri, R. Sordan, C. Spinella, G. Nicotra, Homogeneity of Ge-rich nanostructures as characterized by chemical etching and transmission electron microscopy, Nanotechnology 23 (4) (2012), 045302.

[27] D. Chatain, W.C. Carter, Spreading of metallic drops, Nature Materials, 13(12) (2004), 843-845. DOI: 10.1038/nmat1275.

[28] K. Sudoh, M. Naito, Interfacial reaction during dewetting of ultrathin silicon on insulator, Comptes Rendus Physique 14(7) (2013), 601-606.

[29] Y. Wakayama, T. Tagami, S. Tanaka, Three-dimensional islands of Si and Ge formed on SiO2 through crystallization and agglomeration from amorphous thin films, Thin Solid Films 350.1-2 (1999), 300-307.

[30] R. Tran, Z. Xu, B. Radhakrishnan, D. Winston, W. Sun, K. A. Persson, S. Ping Ong, Surface energies of elemental crystals, Sci Data3 (2016), 160080. https://doi.org/10.1038/sdata.2016.80.

[31] H. S. Chen, D. Turnbull, Specific heat and heat of crystallization of amorphous germanium, Journal of Applied Physics 40.10 (1969), 4214-4215.

[32] A.A. Stekolnikov, J. Furthmüller, F. Bechstedt, Absolute surface energies of group-IV semiconductors: dependence on orientation and reconstruction, Physical Review B 65.11 (2002), 115318.

[33] G. Whyman, E. Bormashenko, T. Stein, The rigorous derivation of Young, Cassie Baxter and Wenzel equations and the analysis of the contact angle hysteresis phenomenon, Chem. Phys. Lett. 450 (2008), 355–359.

[34] R. Sangiorgi, M.L. Muolo, D. Chatain, N. Eustathopoulos, Wettability and work of adhesion of non reactive liquid metals on silica, Journal of the American Ceramic Society 71 (1988), 742-748. DOI: 10.1111/j.1151-2916.1988.tb06407.

[35] F. M. Ross, J. Tersoff, and R. M. Tromp, Ostwald ripening of self-assembled germanium islands on Silicon (100), Microscopy and Microanalysis 4.3 (1998), 254-263.

[36] F. Leroy, Y. Saito, F. Cheynis, E. Bussmann, O. Pierre-Louis, P. Müller, Nonequilibrium diffusion of reactive solid islands, Physical Review B 89.23 (2014), 235406.

[37] F. Leroy, Y. Saito, S. Curiotto, F. Cheynis, O. Pierre-Louis, P. Müller, Shape transition in nano-pits after solid-phase etching of SiO_2 by Si islands, Applied Physics Letters 106.19 (2015), 191601.

[38] Almadori, Y., Borowik, Ł., Chevalier, N., Hourani, W., Glowacki, F., & Barbe, J. C. (2016). From Solid-State Dewetting of Ultrathin, Compressively Strained Silicon–Germanium-on-Insulator Films to Mastering the Stoichiometry of Si1–x Ge x Nanocrystals. The Journal of Physical Chemistry C, 120(13), 7412-7420.

[39] Z. Chehadi, M. Bouabdellaoui, M. Modaresialam, T. Bottein, M. Salvalaglio, M. Bollani, D. Grosso, M. Abbarchi, Scalable Disordered Hyperuniform Architectures via Nanoimprint Lithography of Metal Oxides, ACS Applied Materials & Interfaces 13 (31) (2021), 37761–37774.